

Detection of Partial Discharge in An Oil Filled-Tank Using Acoustic in Audio Frequency Range

Mochammad Wahyudi
Department of Electrical and
Information Engineering
Universitas Gadjah Mada
Yogyakarta, Indonesia
mochammadwahyudi@ugm.ac.id

Noor Akhmad Setiawan
Department of Electrical and
Information Engineering
Universitas Gadjah Mada
Yogyakarta, Indonesia
noorwewe@ugm.ac.id

Bambang Sugiyantoro
Department of Electrical and
Information Engineering
Universitas Gadjah Mada
Yogyakarta, Indonesia
bsg@ugm.ac.id

I Made Yulistya Negara
Department of Electrical Engineering
Institut Teknologi Sepuluh Nopember
Surabaya, Indonesia
yulistya@ee.its.ac.id

Gilang Adityasakti
Department of Electrical and
Information Engineering
Universitas Gadjah Mada
Yogyakarta, Indonesia
gilang.adityasakti@mail.ugm.ac.id

Abstract—In this paper, the acoustic signal within an audio sonic range emitted by partial discharge (PD) in an oil-filled cylindrical tank was investigated. The PD was generated by point-to-flat electrodes subjected to a high-voltage DC. The PD source location, installation method, and sensor microphone, as well as the electrode gap distance, were varied. Subsequently, acoustic waveforms and their frequency spectrum, as well as the PD current, were analyzed. The results showed that transient acoustic signals indicated the emergence of PD. The acoustic sensor attached to the outer wall of the tank (contact type) was more sensitive than the sensor that had a distance from the tank (non-contact type). Sensor contact type acoustic signals placed parallel to the location of the PD source provided a more accurate signal form compared to those set nonparallel to the frequency spectrum, which was relatively flat. A closer electrode distance caused the duration, acoustic signal amplitude as well as the currents to be more considerable. For the identical variable, the acoustic signal form was not related to the current signal despite the same signal duration. Besides, locations of sources of the PD notably influenced the signal form, but it did not apply for the current signal.

Keywords—acoustic, audio frequency, fast Fourier transform, high-frequency current transformer, oil transformer, partial discharge

I. INTRODUCTION

Partial discharge (PD) is the beginning of insulation failure. Ironically, PD in power transformer is often ignored. This was indicated by the absence of a PD detection system installed. Consequently, many cases of power outages occur suddenly and unscheduled as the transformer is damaged. Equipment replacement also requires considerable time and cost. Thus, many losses are caused by the absence of a PD detection system at the transformer.

The PD generates several emissions, such as light [1-3], heat [4-6], electromagnetic waves [7,8], and acoustic waves [9-11], as well as current [12,13] so that they can be used as an indicator of PD existence. In this case, the PD detection method is designed by using the characteristic of the emission signal. PD detection in transformer oil has a unique challenge due to its presence inside the transformer's tank.

The use of a high-frequency current transformer (HFCT) sensor will be challenging to determine that PD current pulses are sourced from the transformer oil insulation [1]. In addition, the electromagnetic sensor is vulnerable to noises produced by electromagnetic waves, such as telecommunication signals. Dissolved gas analysis (DGA) is carried out by taking oil samples [2]. It will consume a lot of time, and the results cannot be obtained in real-time.

The acoustic method is resistant to electromagnetic interference. Moreover, its installation in the transformer tank is relatively easy and practical. This method can also provide the results in real-time. On the other hand, acoustic is vulnerable to audible surrounding noises. This problem may be anticipated by using an ultrasonic sensor. But, this sensor with high sensitivity and wide spectrum frequency is relatively much more expensive than another sensor type with the same quality, i.e., microphone sensor (audio frequency range). The weakness of the microphone, as stated before, may be compensated by applying this sensor to the power transformer located in areas that are relatively not crowded all the time or low noises. In addition, artificial intelligence has widely been developed to recognize the different characteristics of sound, so that it can be adopted to mitigate audible noises disturbing PD acoustic signal in the future.

Many detection systems had been designed for the PD in an oil-contained transformer tank with box type [14-18]. This type is, indeed, commonly used in all voltage systems. Otherwise, the PD detection for a cylinder type transformer tank is very little [19]. The cylinder tanks widely used for distributed voltage systems are still commonly found in certain areas, mostly in rural areas. In [19], the PD was generated using a flat-plate needle electrode subjected to a DC voltage. The locations of PD sources were varied, while the sensor locations were not altered (attached to the outer tank wall). The utilized sensor had a frequency width of up to 1000 kHz. The results showed that the acoustic signal emitted by the frequency bandwidth of the detected acoustic signal was affected by the location of the PD source. In this case, the highest peaks were always met at a frequency of less than 100 kHz. In other words, the higher the frequency, the lower the relative amplitude. According to these findings, the use of acoustic sensors in the audio frequency

range for PD detection in a cylindrical tank has good potential to be investigated.

In this study, the acoustic emission characteristics of PD in the audio frequency range in the oil-filled cylinder tank on the given variables were investigated. In this case, the effects of the way a sensor was installed and the location where the microphone sensor was attached as well as the electrode distance toward signal characteristics and acoustic frequency spectrums, were analyzed. High-frequency current sensors were also used; therefore, the correlation between the acoustic signal characteristics and the current could be described.

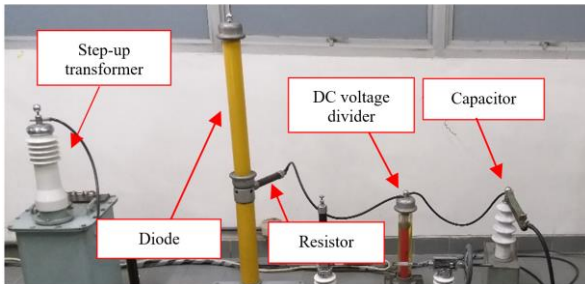


Fig. 1. Configuration of DC high voltage generation system



Fig. 2. Electrode system: flat model (left) and point model (right)



Fig. 3. Configuration of PD generation in oil filled-tank

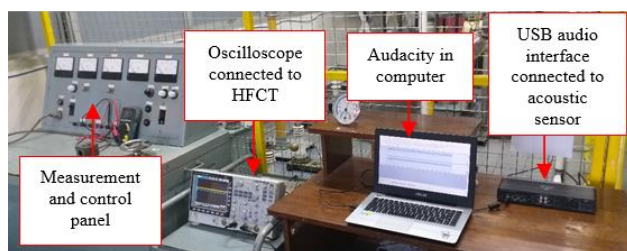


Fig. 4. Configuration of the data acquisition system

II. METHODS

The methods used for an experimental setup in this research will be described in the following points.

A. Configuration of PD Generation System

The DC high voltage generation circuit and the point-to-flat electrodes were needed to generate PD, as shown in Fig. 1 and 2, respectively. The DC high voltage was basically obtained from the AC high voltage rectified by a diode. A step-up transformer provided the AC high voltage with a 220 V: 50 kV ratio. The waveform of the diode output voltage was smoothed by a capacitor (0.1 μ F). In addition, a resistor (50 k Ω) was added to limit PD current peak. The point electrode was subjected to the DC high voltage, while the flat electrode was connected to a grounding system. Both electrodes were immersed in a transformer oil tank, as depicted in Fig. 3. The tank was cylindrical with a diameter of 27 cm and a height of 45 cm. Shell Diala S4 ZX-I was used as the oil transformer.

B. Configuration of PD Detection System

The data acquisition devices configuration is shown in Fig. 4. There were two PD detection methods employed. The first one was based on acoustic as an investigated signal. It consisted of two Behringer ECM8000 measurement condenser microphones, a Behringer UMC404HD audio interface, and Audacity software. The specifications of the Behringer sensor and audio interface are given in Table I and II, respectively. The Behringer ECM8000 was chosen as the acoustic sensor since it had flat frequency response and ultra-high sound resolution. The audio interface had mic preamplifiers. However, in this experiment, it was set at a minimum level. The audio interface accompanied by Audacity was employed to record the acoustic signal. In Audacity, the sample rate of recording was chosen to be 44.1 kHz. This value met the Nyquist's criteria.

The second method was based on high frequency current as a reference signal. It was comprised of an Innovit high frequency current transformer (HFCT) and a GW-Instek GDS-3254 digital oscilloscope. The PD activity would emit small currents with high frequency components. Then, these impulse currents traveled along the grounded cable and passed through the HFCT. The oscilloscope then acquired the HFCT output voltage. The HFCT and oscilloscope specifications are presented in Table III and IV, respectively.

TABLE I. ACOUSTIC SENSOR SPECIFICATION

Parameter	Value
Impedance	200 Ω
Sensitivity	70 dB
Frequency response	20 Hz – 20 kHz
Phantom power	+15 V to +48 V

TABLE II. AUDIO INTERFACE SPECIFICATION

Parameter	Value
Total of input channel	4 channels
Frequency response	10 Hz – 50 kHz (input), 10 Hz – 43 kHz (output)
Supported sample rates	44.1/48/88.2/96/176.4/192 kHz (24 Bit)
Phantom power	+48 V

TABLE III. HFCT SPECIFICATION

Parameter	Value
Bandwidth	0.3 ~ 150 MHz
Sensitivity, current input	1 mA (peak-to-peak)
Sensitivity, voltage output	≥ 16 mV (peak-to-peak)
Load impedance	50 Ω
Hole dimension	54 mm

TABLE IV. DIGITAL OSCILLOSCOPE SPECIFICATION

Parameter	Value
Total of input channel	4 channels
Bandwidth	250 MHz
Real-time sampling rate	5 GSa/s
Rise time	1.4 ns

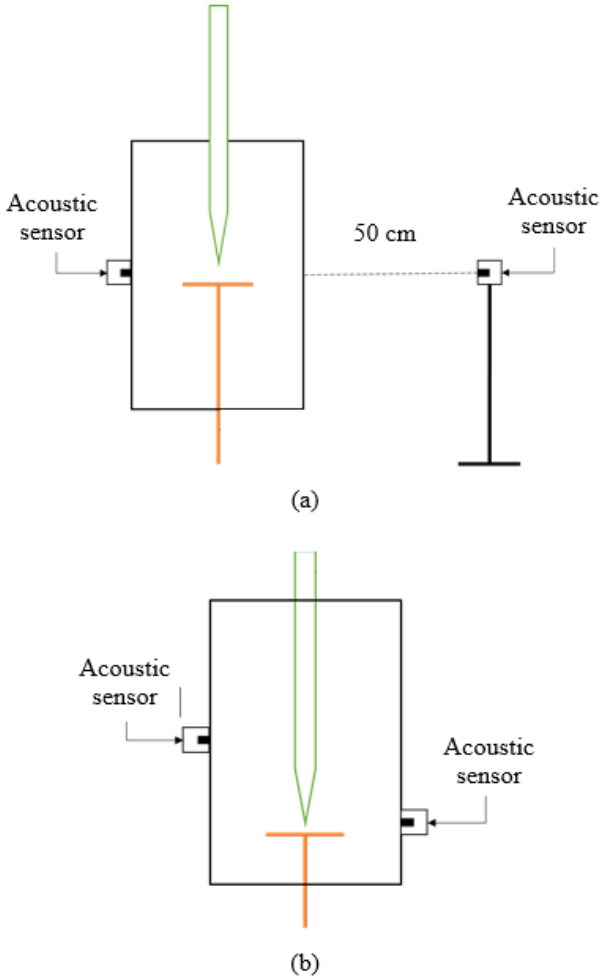


Fig. 5. Location variations of the PD source and acoustic sensors: (a) The first scheme. (b) The second scheme.

C. Scheme of The Experiment

The Positions of electrodes and acoustic sensors were varied, as shown in Fig. 5. In the first scheme, the location of PD was at the tank center (0,0), and there were two differently installed acoustic sensors. The first one touched the outer tank wall (contact type), and the second one did not touch the tank (non-contact type). In the second scheme, the PD position was lowered by 10 cm from the tank center, so that it was at a point (0,-10). The two sensors were contact type, but their position was different. The first one was parallel to the PD source location at point (0,-10), while another sensor was nonparallel to the point (0,0). In

addition, the gap distance between electrodes was varied for all schemes, namely 1 mm and 2 mm.

D. Data Recording and Processing

The DC high voltage applied to the point electrode was increased by 1 kV per step until the PD current was clearly visible on the oscilloscope screen. Along with it, the acoustic sensor output was recorded. Otherwise, the HFCT output was only recorded when the PD current appeared since the oscilloscope recording duration was limited. The recorded acoustic signal in decibels was relative to full scale (dBFS). In the dBFS unit, the loudest sound detectable by the instrument was represented by the value of 0 dBFS. In other words, the more negative the value of dBFS, the lower the sound. The acoustic signal was then transformed using the fast Fourier transform (FFT) to obtain the frequency spectrum. The frequency spectrum window was a rectangular type with a Y-axis unit in dBFS. The acoustic waveforms and their frequency spectrum, as well as the high frequency discharge current, were analyzed and correlated for all schemes.

III. RESULTS AND ANALYSIS

A. Gap Distance and PD Source Location Effects to PD Current Characteristics

The PD currents based on the first scheme (PD source at (0,0)) and the second scheme (PD at (0,-10)) were shown in Fig. 6 and 7, respectively. Current pulses generally characterized the appearance of PD. However, its presence accompanied by the high amplitude, which was several to tens volt indicated that the PD had developed into arc discharge.

The variation of electrode gap distances produced a significant difference in current characteristics. At the same duration, i.e., 3.5 seconds, the current pulses for the 1 mm gap distance was much more significant and longer than the 2 mm gap distance. In other words, the shorter the gap, the higher the PD activity. These characteristics were found not only in the first scheme but also in the second scheme. Besides that, at the same electrode distance but different PD source positions, the shape of the current pulses was relatively similar. It meant that the PD source position did not affect the current characteristics.

B. First Scheme: Different Sensor Installation Effect (Contact and Non-Contact Type) to Acoustic Characteristics

The acoustic signals for each variation of sensor installation are illustrated in Fig. 8 - 12. The signal emitted by PD was generally characterized by impulse waveform, followed by small distorted waves. In addition, based on the frequency spectrum, the PD appearance was confirmed by a significant increase in amplitude for all audio frequencies.

The contact type acoustic sensor that was attached to the outer wall of the tank had better sensitivity than the non-contact type installed about 50 cm from the outer wall of the tank. At the same duration and gap distance, the sensor with contact type is able to get more acoustic signals (in amplitude and duration) than the non-contact type, as seen in Fig 8(a), 9(a), 10(a), and 11(a). Moreover, the contact type is able to detect earlier, as seen in Fig. 12. In this case,

the contact sensor received the signal 0.0004 s faster than the non-contact sensor.

The impulse waveforms encountered in this scheme may be grouped into two types. The first one is the impulse wave that is sequentially arranged from the valley, the hill, and the valley, as seen in Fig. 8(a), 9(a), and 10(a). In other words, these waveforms were observed on the experiments using the contact type sensor for all gap distance variations and non-contact type sensors for a 1 mm gap distance. The second one is the impulse wave consisted only of the valley, as seen in Fig. 11(a). This waveform was obtained during the experiment using a non-contact sensor for a 2 mm gap distance. In the frequency spectrum, the first type gave a relatively regular and smooth curve, while the second type resulted in a curve that had a lot of high peaks and was irregular.

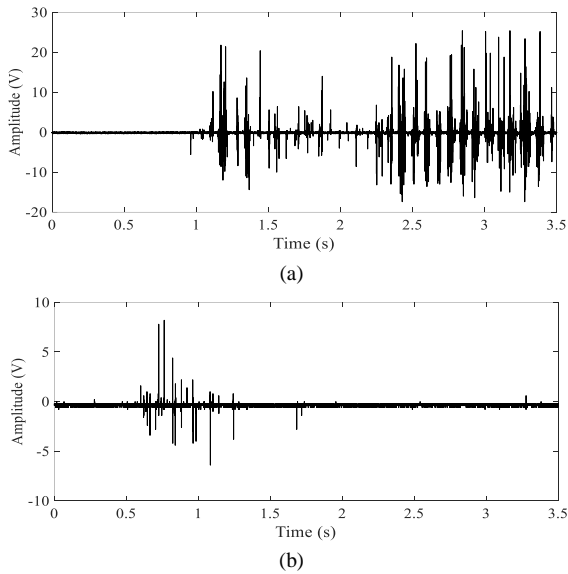


Fig. 6. Current pulses during the first scheme with different gap distances: (a) 1 mm. (b) 2 mm.

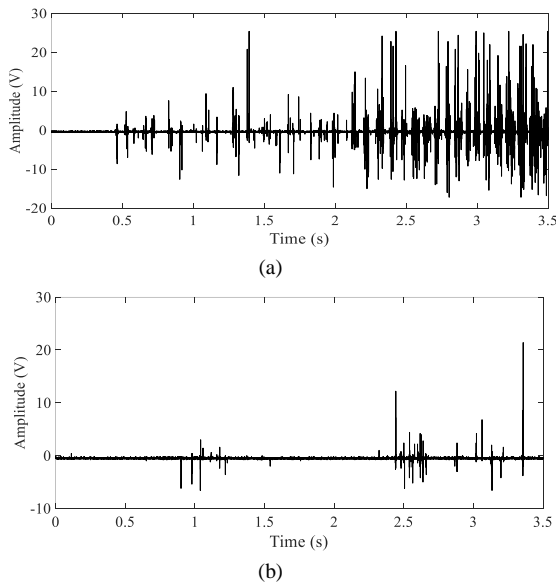


Fig. 7. Current pulses during the second scheme with different gap distances: (a) 1 mm. (b) 2 mm.

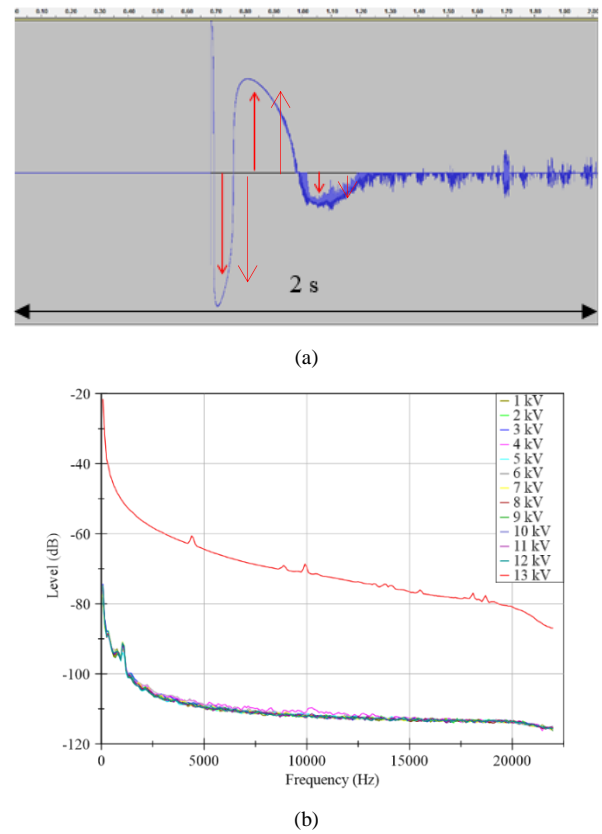


Fig. 8. Acoustic characteristics based on a contact type sensor and a 1mm gap distance. (a) PD acoustic signal (13 kV). (b) The frequency spectrum of non-PD (1 kV - 12 kV) and PD (13 kV).

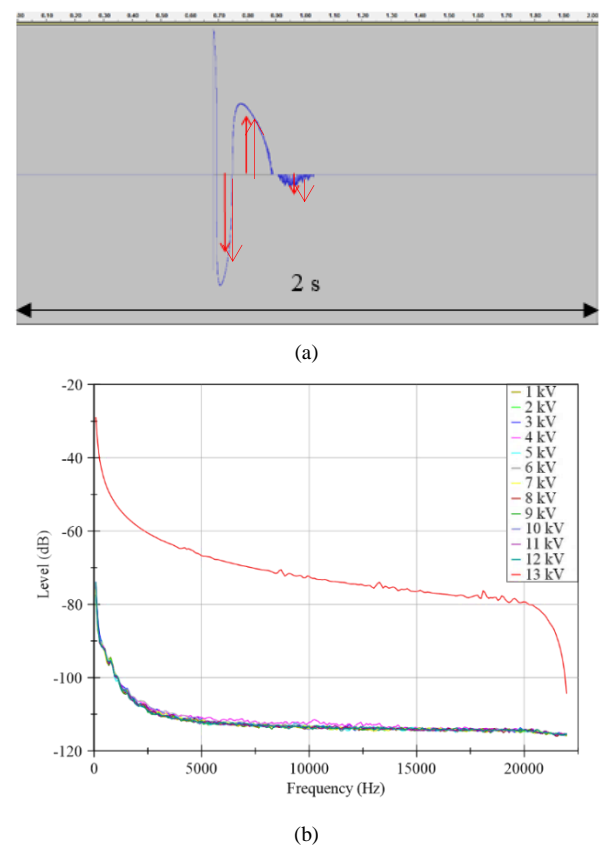
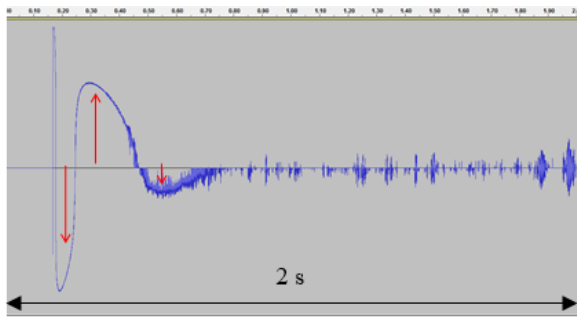
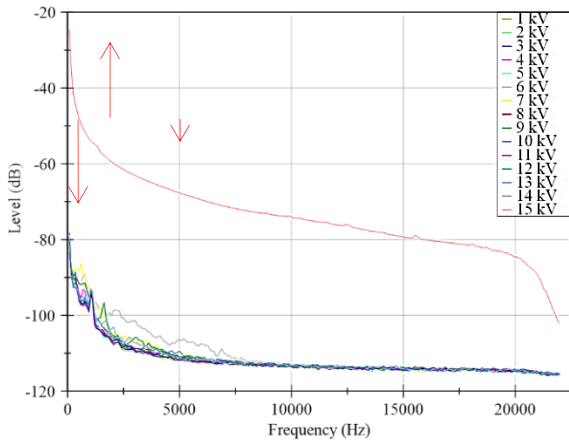


Fig. 9. Acoustic characteristics based on a non-contact type sensor and a 1 mm gap distance. (a) PD acoustic signal (13 kV). (b) The frequency spectrum of non-PD (1 kV - 12 kV) and PD (13 kV).

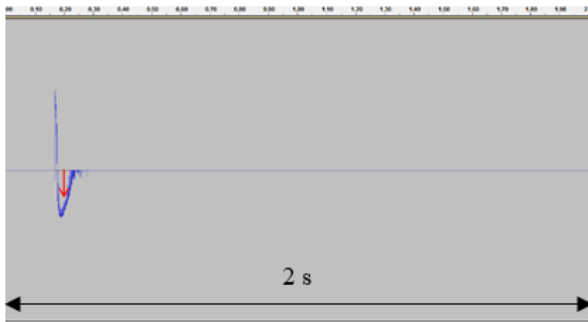


(a)

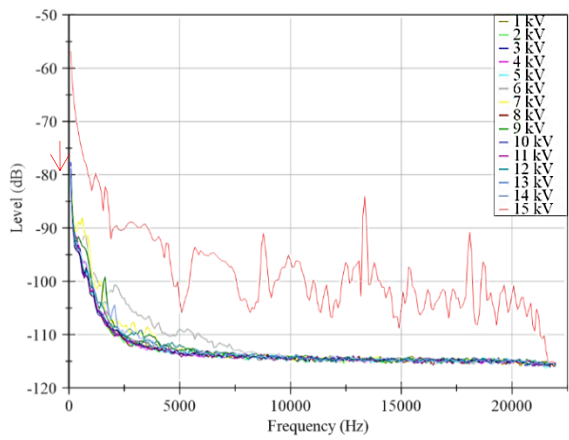


(b)

Fig. 10. Acoustic characteristics based on a contact type sensor and a 2 mm gap distance. (a) PD acoustic signal (15 kV). (b) The frequency spectrum of non-PD (1 kV - 14 kV) and PD (15 kV).

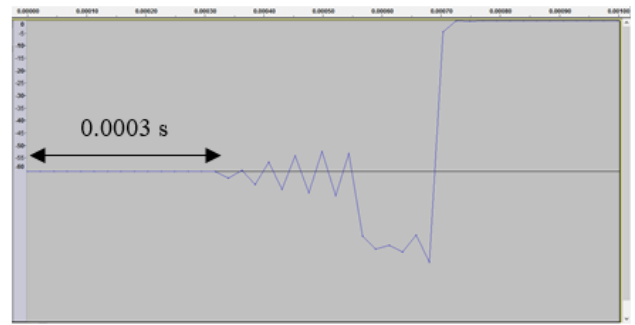


(a)

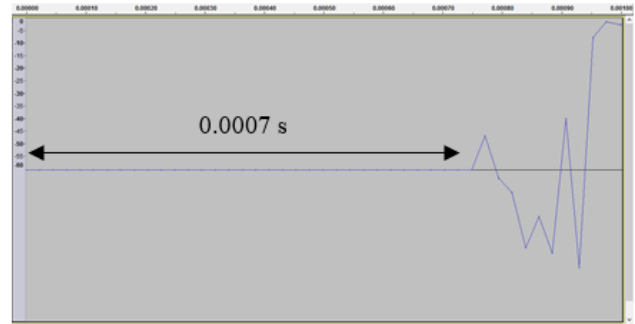


(b)

Fig. 11. Acoustic characteristics based on a non-contact type sensor and a 2 mm gap distance. (a) PD acoustic signal (15 kV). (b) The frequency spectrum of non-PD (1 kV - 14 kV) and PD (15 kV).



(a)



(b)

Fig. 12. Difference in sensor sensitivity: (a) Contact type. (b) Non-contact type.

C. Second Scheme: Effect of Different Mounting Position (Contact Type) to Acoustic Characteristics

The acoustic signals based on contact type sensors installed with various positions, i.e., parallel and nonparallel to the PD source location, are shown in Fig. 13 – 15. The experiment using a sensor parallel to the PD source location for all gap distance variations shows the first type of impulse waveform sequentially composed of the valley, the hill, and the valley, as illustrated in Fig. 13(a) and 15(a). On the other hand, the experiment using a nonparallel sensor exhibits two different waveforms, namely the second type impulse, which is only structured from the valley, as seen in Fig. 14(a), for a 1 mm gap distance, and the distorted non-impulse, as seen in Fig. 16(a), for a 2 mm gap distance. In addition, the amplitude of the parallel sensor is higher than the nonparallel sensor. The second type impulse and the non-impulse type cause the curve of the frequency spectrum to be irregular and have many high peaks. It is very different from the first type.

D. Correlation Between Acoustic and PD Current Signal

The waveforms comparison between the acoustic and the current at the same PD position and gap distance are illustrated in Fig. 17 - 20. The acoustic and current waveforms do not depend on each other. These results strongly prove that the acoustic signal is not generated by the PD current, and vice versa. On the other hand, the duration of acoustic and current signals is relatively the same. It confirms that the detected acoustic signals are the PD emission. Moreover, both signals have a longer duration in the experiment with the 1 mm gap distance than the 2 mm gap distance. The signal sensitivity difference could not be analyzed since the acoustic signal and current

were not acquired by the same device (synchronization could not be performed).

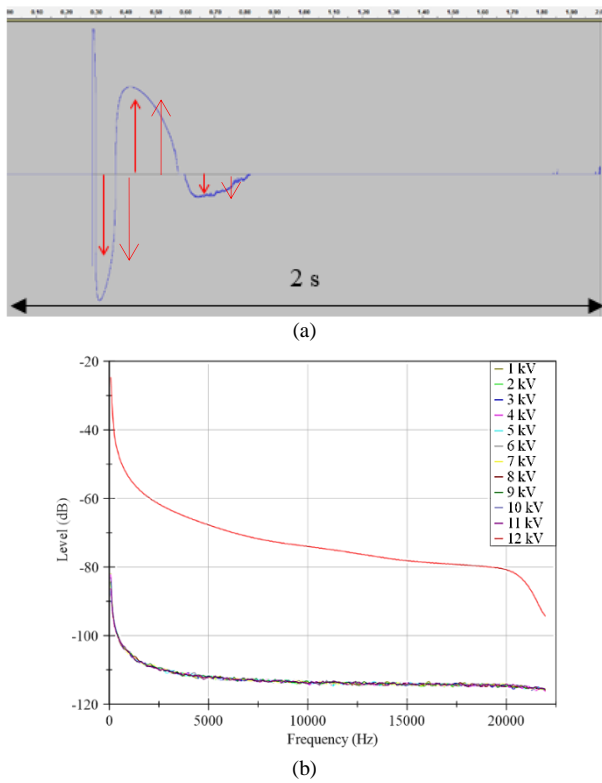


Fig. 13. Acoustic characteristics based on a 1 mm electrode gap and contact type sensor parallel to the PD source location. (a) PD acoustic signal (12 kV). (b) The frequency spectrum of non-PD (1 kV - 11 kV) and PD (12 kV).

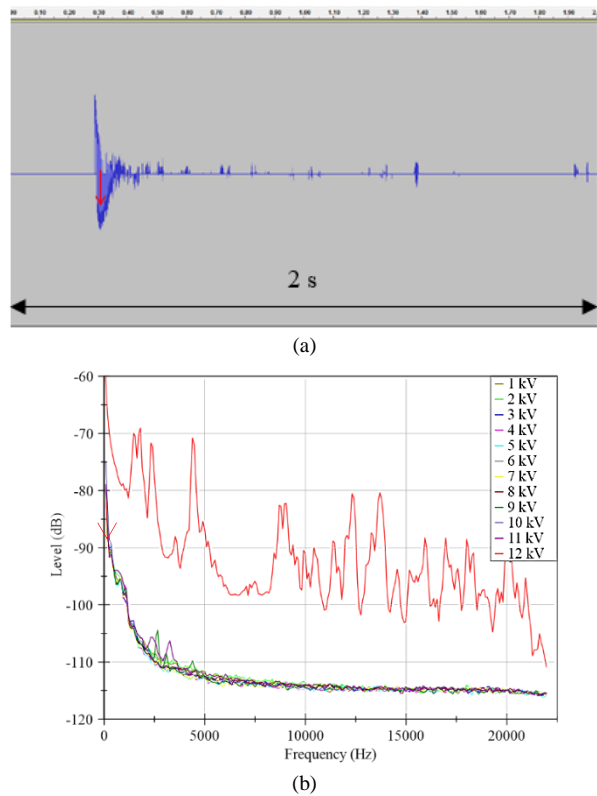


Fig. 14. Acoustic characteristics based on a 1 mm electrode gap and contact type sensor nonparallel to the PD source location. (a) PD acoustic signal (12 kV). (b) The frequency spectrum of non-PD (1 kV - 11 kV) and PD (12 kV).

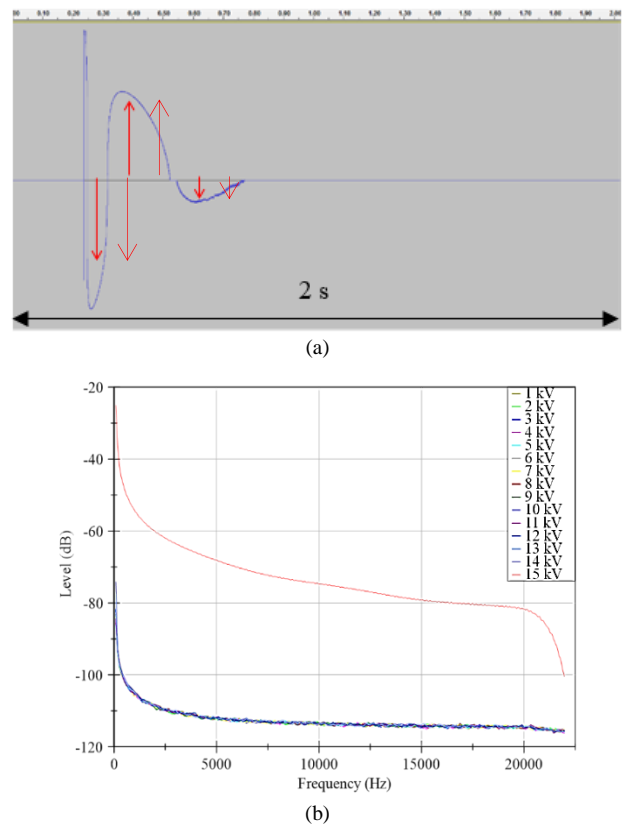


Fig. 15. Acoustic characteristics based on a 2 mm electrode gap and contact type sensor parallel to the PD source location. (a) PD acoustic signal (15 kV). (b) The frequency spectrum of non-PD (1 kV - 14 kV) and PD (15 kV).

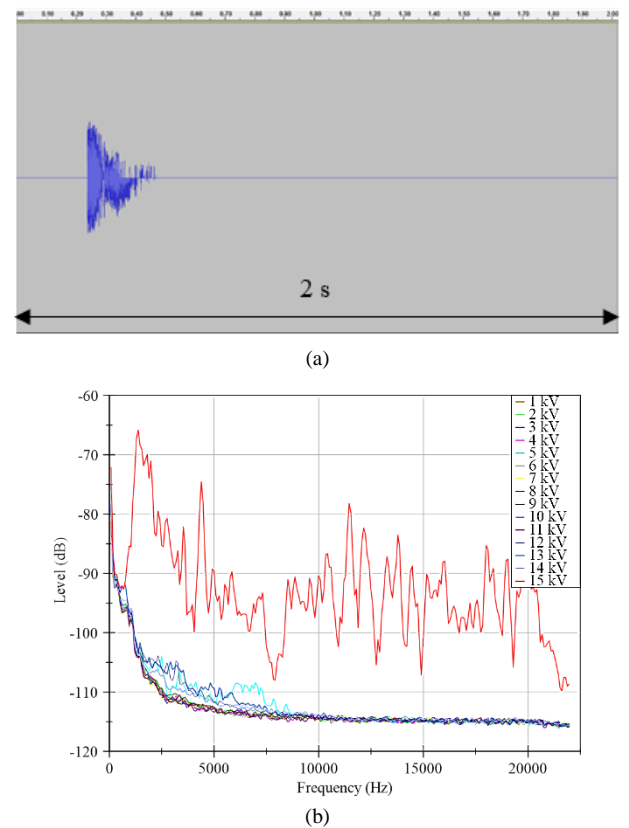
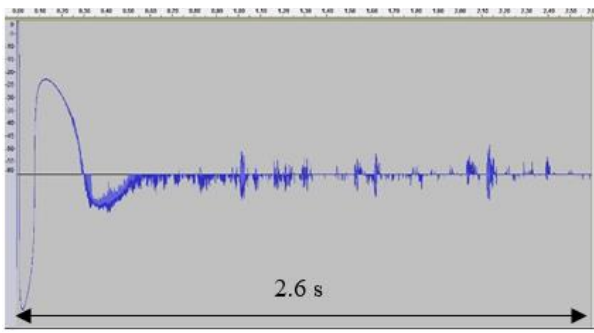
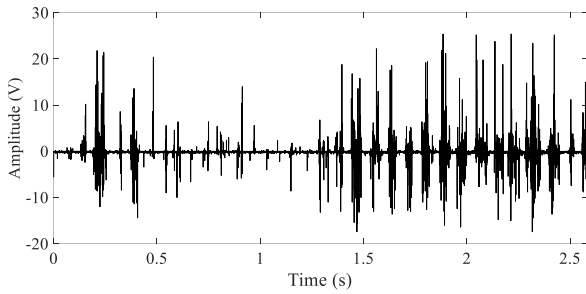


Fig. 16. Acoustic characteristics based on a 2 mm electrode gap and contact type sensor nonparallel to the PD source location. (a) PD acoustic signal (15 kV). (b) The frequency spectrum of non-PD (1 kV - 14 kV) and PD (15 kV).

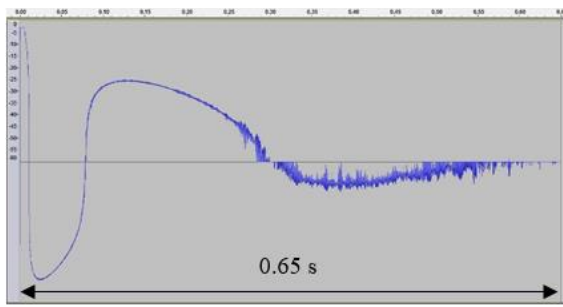


(a)

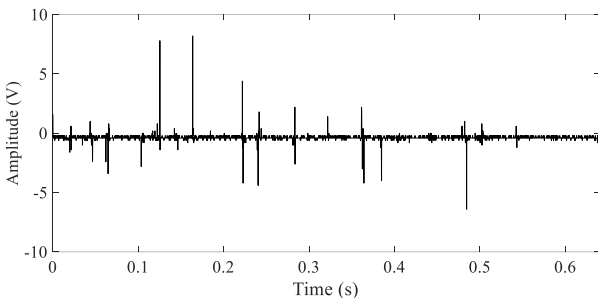


(b)

Fig. 17. Results based on PD position at (0,0) and a 1 mm gap distance: (a) Acoustic signal for contact type. (b) Current signal.

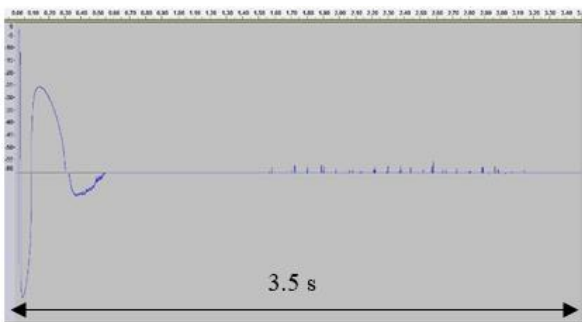


(a)

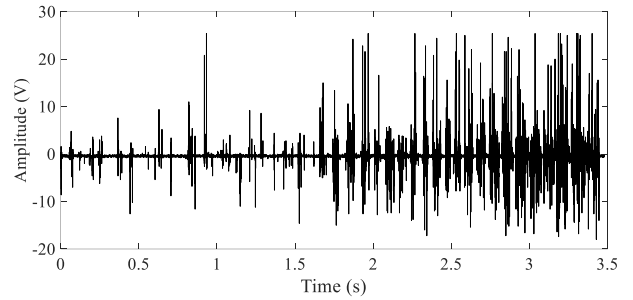


(b)

Fig. 18. Results based on PD position at (0,0) and a 2 mm gap distance: (a) Acoustic signal for contact type. (b) Current signal.

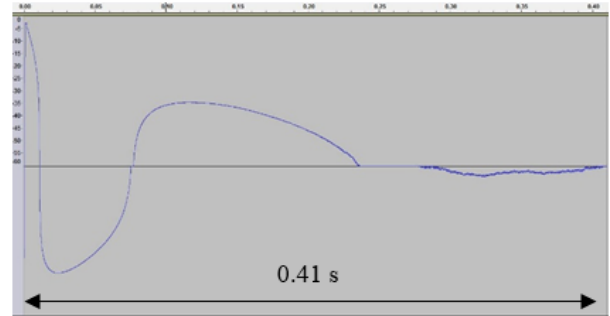


(a)

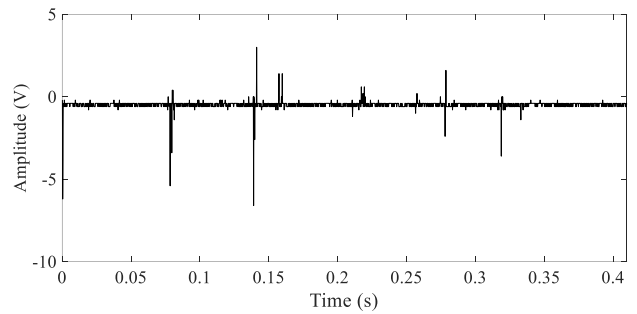


(b)

Fig. 19. Results based on PD position at (0,-10) and a 1 mm gap distance: (a) Acoustic signal for contact type. (b) Current signal.



(a)



(b)

Fig. 20. Results based on PD position at (0,-10) and a 2 mm gap distance: (a) Acoustic signal for contact type. (b) Current signal.

IV. CONCLUSIONS

This experiment has been able to generate PD in an oil-filled tank and to detect its acoustic emission in audio frequency. The presence of PD has successfully been validated by the high frequency current pulses. The high amplitude of current pulses indicates that the PD has developed into arc discharge. Based on the acoustic signal, the PD condition is characterized by the existence of transient waveforms. They are the impulse and highly distorted non-impulse types. The acoustic sensor attached to the outer wall of tank (contact type) is more sensitive than the sensor that has a distance from the tank (non-contact). The contact type sensor installed parallel to the PD source location resulted in the impulse waveform that was more accurate than the nonparallel contact sensor. This indicates that the perfection level of impulse waveform may reveal the PD location in the oil-filled tank. The acoustic and current waveforms do not depend on each other. However, the closer electrode gap distance equivalently causes longer acoustic and current duration. In addition, the current is not influenced by the PD source location.

REFERENCES

- [1] S. M. Brahma, Youngseok Kim, Kilmok Shong, "The Characteristics of UV Strength According to Corona Discharge From Polymer Insulators Using a UV Sensor and Optic Lens", *IEEE Transactions on Power Delivery*, Vol. 26, Issue 3, pp. 1579 – 1584, July 2011.
- [2] N. Maistry, RA. Schutz, E. Cox, "The Quantification of Corona Discharges on High Voltage Electrical Equipment in the UV Spectrum using a Corona Camera", 2018 International Conference on Diagnostics in Electrical Engineering (Diagnostika), Pilsen, Czech Republic, September 4-7, 2018
- [3] Li Yongxiang, Wang Tianzheng, Guo Liqiang, Wang Zhipeng, Guo Ting, Cheng Xueting, "Detection and analysis of high voltage electrical equipment corona discharge based on ultraviolet imaging technology", 2017 29th Chinese Control And Decision Conference (CCDC), Chongqing, China, May 28-30, 2017
- [4] B. X. Du, Meng Xiao, "Thermal Accumulation and Tracking Failure Process of BN-filler Epoxy-matrix Composite", *IEEE Transactions on Dielectrics and Electrical Insulation*, Vol. 20, Issue 6, pp. 2270 – 2276, December, 2013
- [5] Shane Morrison, Joni Kluss, John Ball, Lucas Cagle, Sam Bryan, "Thermal Imaging for Rapid Noninvasive On-site Insulation Diagnostics", 2019 IEEE Electrical Insulation Conference (EIC), Calgary, AB, Canada, Canada, June 16-19, 2019
- [6] Siyuan He, Dawei Yang, Wentao Li, Yong Xia, Yandong Tang, "Detection and fault diagnosis of power transmission line in infrared image", 2015 IEEE International Conference on Cyber Technology in Automation, Control, and Intelligent Systems (CYBER), Shenyang, China, June 8-12, 2015
- [7] Yuda Muhammad Hamdani, Umar Khayam, "Application of Ultra-Wideband Double Layer Printed Antenna for Partial Discharge Detection", 2018 5th International Conference on Electrical Engineering, Computer Science and Informatics (EECSI), Malang, Indonesia, October 16-18, 2018
- [8] Umar Khayam, F. I. Fatoni, "Design and application of loop antenna for partial discharge induced electromagnetic wave detection", 2017 6th International Conference on Electrical Engineering and Informatics (ICEEI), Langkawi, Malaysia, November 25-27, 2017
- [9] IEEE Guide for the Detection, Location and Interpretation of Sources of Acoustic Emissions from Electrical Discharges in Power Transformers and Power Reactors, IEEE Power and Energy Society, IEEE Std C57.127™-2018
- [10] Ran Duan, Guanghao Xu, Ming Ren, Ming Dong, Xuze Gao, Changjie Xia, "Multi-band Ultrasonic Detection Analysis of the Evolution Process of Point Discharge Under Power Frequency Voltage", 2019 IEEE Conference on Electrical Insulation and Dielectric Phenomena (CEIDP), Richland, WA, USA, USA, October 20-23, 2019
- [11] Li Yanqing, Lu Fangcheng, Xie Hongling, Wang Yongqiang, "Study on ultrasonic generation mechanism of partial discharge", Proceedings of 2005 International Symposium on Electrical Insulating Materials, 2005. (ISEIM 2005), Kitakyushu, Japan, June 5-9, 2005
- [12] F. Álvarez, E. Arcones, F. Garnacho, A. Ramírez, J. Ortego, "Efficient PD Monitoring of HV Electrical Systems Using HFCT Sensors", 2018 IEEE International Conference on High Voltage Engineering and Application (ICHVE), ATHENS, Greece, Greece, September 10-13, 2018
- [13] J. Singsathien, T. Suwanasri, C. Suwanasri, S. Ruankon, P. Fuangpian, W. Namvong, P. Saengsaikaew, W. Khotsang, "Partial discharge detection and localization of defected power cable using HFCT and UHF sensors", 2017 14th International Conference on Electrical Engineering/Electronics, Computer, Telecommunications and Information Technology (ECTI-CON), Phuket, Thailand, June 27-30, 2017
- [14] Seyed Amir Mahmood Najafi, Hassan Saadati, Peter Werle, "Comparison of acoustical partial discharge signals under AC and DC," *IEEE Electrical Insulation Conference (EIC)*, Montreal, Qc, Canada, pp. 523-526, June 2016.
- [15] Gyung-Suk Kil, Il-Kwon Kim, Dae-Won Park, Su-Yeon Choi, Chan-Young Park, "Measurements and analysis of the acoustic signals produced by partial discharges in insulation oil," *Jurnal of Current Applied Physics* 9, pp. 296-300, 2009.
- [16] Arsalan Hekmati, "A novel-acoustic method of partial discharge allocation considering structure-borne waves," *Journal of Electrical Power and Energy Systems* 77, pp. 250-255, 2015.
- [17] Hua-Long Liu, "Acoustic partial discharge localization methodology in power transformers employing the quantum genetic algorithm," *Journal of Applied Acoustics* 102, pp. 71-78, 2016.
- [18] Arsalan Hekmati, "Proposed method of partial discharge allocation with acoustic emission sensors within power transformers," *Journal of Applied Acoustics* 100, pp. 26-33, 2015.
- [19] Sakoda, T. Arita, H. Nieda, K. Ando, "Analysis of Acoustic Emissions Caused by the Partial Discharge in the Insulation Oil", Proceedings of 13th International Conference on Dielectric Liquids (ICDL '99), Nara, Japan, July 20-25, 1999.